Influence of the characteristics of the implant on the stress distribution of the humerus after a shoulder resurfacing arthroplasty

Daniela Filipa Guerra Burrinha
MSc in Biomedical Engineering
Instituto Superior Técnico
daniela.burrinha@tecnico.ulisboa.pt

Abstract: The shoulder resurfacing arthroplasty has been gaining popularity as an alternative to conventional shoulder arthroplasty surgery due to its several advantages, such as, high bone stock preservation and ease of revision. Nonetheless, the implantation of a prosthesis affects the natural loading distribution in the bone which is likely to cause and adverse bone remodeling. The main goal of this work is to understand the influence of the characteristics of the prosthesis on the stress and strain distribution patterns in the humerus after a shoulder resurfacing arthroplasty. In order to do so, five prostheses were modeled: a standard model, currently in use, two models with a larger and a thinner stem, and two models with a longer and a smaller stem. The implantation of all these models was virtually simulated for five subjects. Finite element models were developed to analyze the loading distribution in the bone considering muscle and joint reaction forces for an abducted and flexed position of the upper limb. The different models were evaluated regarding the Von Mises stress and the strain energy density values. The results obtained are consistent with the literature, i.e., stress shielding occurs when a resurfacing arthroplasty is performed. The results indicate that a prosthesis with a thinner stem minimizes the differences in stress and strain patterns between the intact bone and the implanted bone. However, this study focused only on stress shielding and other key factors, such as the mechanical stability, must also be addressed in future studies.

Keywords: Shoulder joint, Shoulder resurfacing arthroplasty, Stress shielding, Strain shielding, Finite element analysis.

1. Introduction

The shoulder arthroplasty which consists in the substitution of the shoulder joint by an implant is an efficient treatment indicated for several shoulder pathologies. In spite of its favorable outcomes, it is associated with complications that may compromise the results, such as loosening and periprosthetic fracture (Wirth and Rockwood Jr. 2017).

Nowadays, the most commonly performed procedures for shoulder replacement are the anatomic shoulder arthroplasty (TSA) and the reverse total shoulder arthroplasty (RTSA). The TSA tries to reconstruct closely the native anatomy of the shoulder. For patients with a rotator cuff pathology, RTSA is recommended as it provides the stability needed by fixing the joint center of rotation on the scapula.

The shoulder arthroplasty has become an option not only for an elderly population but also for younger and more active patients (Widnall et al. 2013). New implant designs and materials are being studied to achieve better implant performance and outcomes, resulting in a reduced need for revision surgery.

Over the past years, the shoulder resurfacing arthroplasty (SRA) has gained popularity as an alternative to conventional shoulder arthroplasty (Burgess et al. 2009). The SRA presents several advantages being the high bone stock preservation the most relevant, especially in younger patients who may need further arthroplasty procedures (Rai et al. 2016; Schmidutz et al. 2014; Widnall et al. 2013).

Several studies on the short and long term results have shown optimistic functional results for the SRA, but it is also acknowledged that the type of implant used affects the natural stress distribution in the bone and leads to an undesirable stress shielding effect (Schmidutz et al. 2014).

Considering that variations of stem length and diameter in hip resurfacing prostheses led to different stress shielding patterns (Rothstock et al. 2011), the main goal of this work is to evaluate the difference of these characteristics in loading distribution of the humerus after an SRA using three-dimensional finite element models. Five resurfacing prosthesis models with different stem diameter and length are analyzed for five subjects.

2. Materials and Methods

Computational Modeling Pipeline

The computational work behind the models follows an extensive pipeline of actions, based on the work of Ribeiro et al. (2009), resumed in Figure 1. The used methodology that follows this pipeline will be addressed in detail. The geometries were obtained through a set of

Computational Tomography (CT) scans from five different subjects.

Figure 1 - Software pipeline followed: Task, Tool, and Extension.

Image Segmentation, Correction and Final Geometry

In this study ITK-SNAP was used to segment structures in 3D medical images. This software used an active contour method through thresholding to build a semi-automatic segmentation image, and then a manual delineation was made to correct imperfections.

After this process finished a filter correction on the whole geometry was applied using Meshlab® to smooth staircase effects.

The CT images used did not have the same size or resolution and the scans were oriented to different pathologies. For that reason, the scans did not cover the diaphysis of the humerus evenly to every subject. In order to obtain uniformity between subjects, an artificial elongation of the diaphysis was performed on Solidworks®

Prostheses Design and Implantation

The rationale behind the different parameters that were studied was to change the length and width of the stem relatively to the standard prosthesis. The prosthesis in which this study is inspired is a Global CAP commercialized by DePuy Synthes. The model is available in different sizes conjugating different head height and head diameter combinations.

Using Solidworks® a model inspired in this resurfacing prosthesis was created, this model will be addressed as the “standard model” depicted in Figure 2.

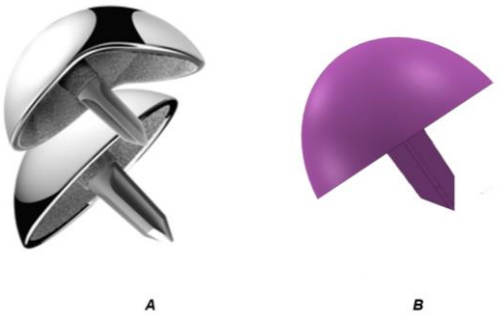

Figure 2 - Global CAP prosthesis normal design and design with increased area of superolateral articulation (A) (DePuy Synthes 2017) and designed model (B).

The parameter variations performed consisted in (1) decrease and increase of 25% in stem diameter, or (2) decrease and an increase of 25% in stem length. This process resulted in four different models which will be further addressed as thinner, larger, smaller, and longer.

The difference between models are depicted in Figure 3.

All modifications were performed from the standard model, which in turn, was designed choosing the best combination of head height and head diameter for each individual.

Figure 3 - Thinner model, Larger model, Standard model, Smaller model, Longer model.

The SRA was simulated for all implants by following the surgical technique provided by the DePuy Synthes (DePuy Synthes 2017).

Physical Properties

Bone was considered an isotropic, linearly elastic material**.** The mechanical properties of the bone tissue follow Gupta and Dan (2004) work which relates Young’s Modulus with density by the equations below,

$$E = 1049.25 \times 10^{-6} \times \rho^2,\ \rho \leq 350\ kg.m^{-3} \quad (1)$$

$$E = 3 \times 10^{-6} \times \rho^3, 350 \leq \rho \leq 1800\ kg.m^{-3} \quad (2)$$

where, E represents the Young’s Modulus of each node with a respective density of ρ. The Poisson’s ratio was set to 0.3 for all the domain.

The values of density in the bone came from the CT scans. Using Bonemapy, an Abaqus® plug-in, the original Hounsfield Unit (HU) values from CT scans were assigned to mesh nodes. According to Gupta and Dan (2004), the apparent density ρ can be computed from the CT values, in HU, using a linear calibration derived from two reference points from the CT-scan slices. The first point used as reference is the value of air, which represents non-bone condition which should correspond linearly to the minimum HU value. The second point was the HU of cortical bone which in turn corresponds to the maximum HU value.

For the subjects whose humerus were artificially elongated, a different procedure was followed. As this subjects were artificially elongated the bone geometry was outside of the CT domain and Bonemapy was unable to compute the HU values. A mapping algorithm was built in Matlab® for these cases. Considering the density values from the bone without the artificial elongation and the coordinates of booth the original and elongated humerus as input, the mapping process of the nodes shared between the original and the elongated bones consisted in finding the nodes from the original bone closest to each node in the elongated bone. For each one of these nodes, the density assigned was based on an

inverse distance weighting method. Regarding the nodes in the mesh that were not shared by both the normal and the elongated bone mesh, the mapping act as a projection in the diaphysis direction in order to reproduce the intramedullary canal of the humerus. An illustration of the resulting density distribution for one of the subjects can be seen in Figure 4.

The head of the prosthesis is composed of a Cobalt-Chromium-Molten alloy (CrCoMo), whereas the stem is made of Ti6Al4V, a titanium-aluminum-vanadium alloy. These materials were assigned to a Young's Modulus of 241 GPa and 120 GPa, respectively.

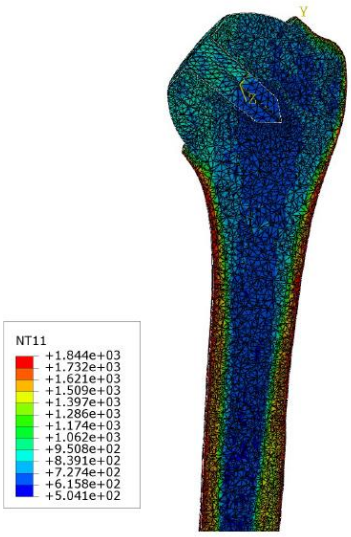

Figure 4 - Example of bone density distribution (kg.m^{-3}) on the bones.

Loading Conditions

Muscular Attachments

With the aim of increasing the accuracy of the analysis, several muscular attachments were simulated in the bone. Nine muscular insertions were created: Supraspinatus, Subscapularis, Pectoralis Major, Latissimus Dorsi, Teres Major, Deltoid, Coracobrachialis, Infraspinatus, and Teres Minor and two muscular origins: Biceps and Triceps. These muscle forces reproduce more truthfully the real dynamic action on the humerus on both load case studies. The muscle attachments were designed directly on each bone following Netter's Atlas of Anatomy (Netter 1989) with the help of a partition tool on Abaqus®

Forces

The data regarding the magnitude of muscle forces and the GH joint reaction force were obtained using the multibody musculoskeletal model of the upper body developed by Quental et al. (2013). The forces applied were computed through inverse dynamics for flexion and abduction positions of 110º.

In order to apply the forces adequately, a Matlab® routine was used to create a unique common referential for every subject and transformed the forces from Quental et al. (2013) in the appropriate coordinate system that was shared by each individual. The common coordinate system is defined as follows:

• Origin – center of the humeral head, computed by fitting a sphere to the humeral head.

• Y-axis – aligned with the diaphysis of the humerus, which is estimated by fitting a cylinder to the diaphysis.

• X-axis – Perpendicular to the plane containing the y-axis and the origin.

• Z-axis – Perpendicular to the x and y-axes.

The application point of these forces is the centroid of each muscular attachment, defined in the form of a Reference Point. Since muscles are not acting on a single point but, instead, on a certain area, the force application point for each muscle was coupled to the attachment area through a Coupling constraint in Abaqus®. The force was distributed considering a uniform distribution.

Regarding the glenohumeral (GH) joint reaction forces, a Matlab® routine was developed to select the nodes on the humeral head surface on which the force was to be distributed. The selection of nodes was based on the projection of the GH reaction force from the joint center to the humeral head surface. A quadratic force distribution was considered (Lacroix, Murphy, and Prendergast 2000).

Modeling Conditions

The final geometry of the models was exported to Abaqus® where it was posteriorly meshed with a quadratic tetrahedral finite element mesh with an edge size of 2 mm. A previous study of results' sensitivity was conducted in order to choose the best type of element and size to this problem.

The interaction between the prosthesis and the bone was modeled accordingly to the different components of the prosthesis. The Global CAP prosthesis has a superficial HA coating on the inner part of its head. This coating promotes bone ingrowth and, at a later stage after implantation, it should be completely fixed to the bone. For that reason, a tie constraint was defined between the prosthesis surface and the bone surface in this area. The stem of the prosthesis, however, is not coated. Since this prosthesis is meant to be used only in uncemented surgeries a contact condition with a small sliding formulation was defined between the surface of the stem and the bone surface within the cut.

The base of the humerus was fixed by a boundary condition of the type Encastre.

Overall, a total of thirty finite element models (FEM) were generated. For each subject in this study, a FEA was performed: (1) the bone implanted without the implant, (2) the bone with the normal prosthesis (3) the bone implanted with the larger prosthesis, (4) the bone implanted with the thinner prosthesis, (5) the bone implanted with the longer prosthesis, (6) and the bone implanted with the smaller prosthesis. The loads, boundary conditions, and other parameters remained unchanged for all simulations.

Results Analysis

The Von Mises stress and strain energy density for the bone were evaluated.

In the quantitative analysis using Equation 3, the bone was divided into eight regions based on the work of Schmidutz et al. (2014). The bone was first divided by a plane passing through the base of the prosthesis' head. Second and third planes divided the bone following the cross on the stem of the prosthesis. This division is made on the humeral head until the most extreme stem length modeled. These regions are depicted in Figure 5.

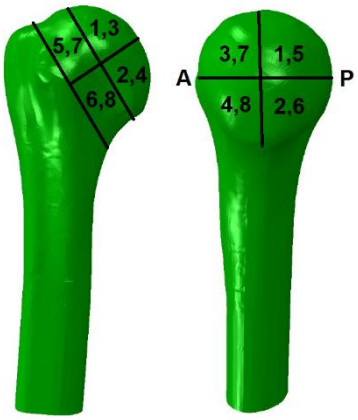

Figure 5 - Regions of the humeral head in the analysis (A – anterior; P – posterior).

This analysis focused on a comparison between the intact bone and the implanted bone for each prosthesis model. For that purpose, a mapping algorithm, similar to the one presented for density mapping, was used to map the Von Mises stress and the strain energy density from the intact bone (IN) to the implanted bone (IM). For each subject, prosthesis, and region, a relative difference between the implanted bone and the intact bone was computed as:

$$\Delta M\ (\%) = \frac{\sum_{i=1}^{n}(M_{IM} - M_{IN}) \times w_i}{\sum_{i=1}^{n} M_{IN} \times w_i} \times 100 \qquad (3)$$

Where ΔM is any one of the physical quantities analyzed, w_i is the volume associated with of the node, a value obtained through the Abaqus® results that acts as a weighting factor, i and n are the total number of nodes in the region under analysis. With these results, a comparison between subjects was made in order to evaluate subject intra-variability in different regions. An inter-variability study was also performed to evaluate the fundamental goal of this work which is to find differences between prostheses modeled. Additionally, a relative difference between the changed implant and the original implant was computed for each region and each subject, i.e.,

$$\Delta V\ (\%) = \frac{\sum_{i=1}^{n}(V_{CM} - V_{SM})}{\sum_{i=1}^{n} V_{SM}} \times 100 \qquad (4)$$

where V_{CM} and V_{OM} represent the quantities compared in the changed model and standard model, respectively.

3. Results

The results were analyzed in three different sections, which consist in (1) qualitative results comparing the intact bone and the implant bone, (2) quantitative results comparing the intact bone and the implant bone, and (3) quantitative results concerning prostheses variability

Intact bone and implanted bone

The results of the intact bone, in Figure 6, show high stresses near the application of the GH joint reaction force and the cortical layer of the diaphysis. In general, the stresses are higher for the abduction movement. For the sake of briefness, and because the results are qualitatively similar for all subjects, and both loading cases, only the results for one subject, S2, for a flexion movement regarding Von Mises Stress are shown.

The introduction of the implant shows a clear reduction of the stresses in the bone, especially in the most superficial regions. In the tip of the stem, the stresses become closer to those found in the intact bone.

The bone area in contact with the rim of the prosthesis shows high values of tension for both movements.

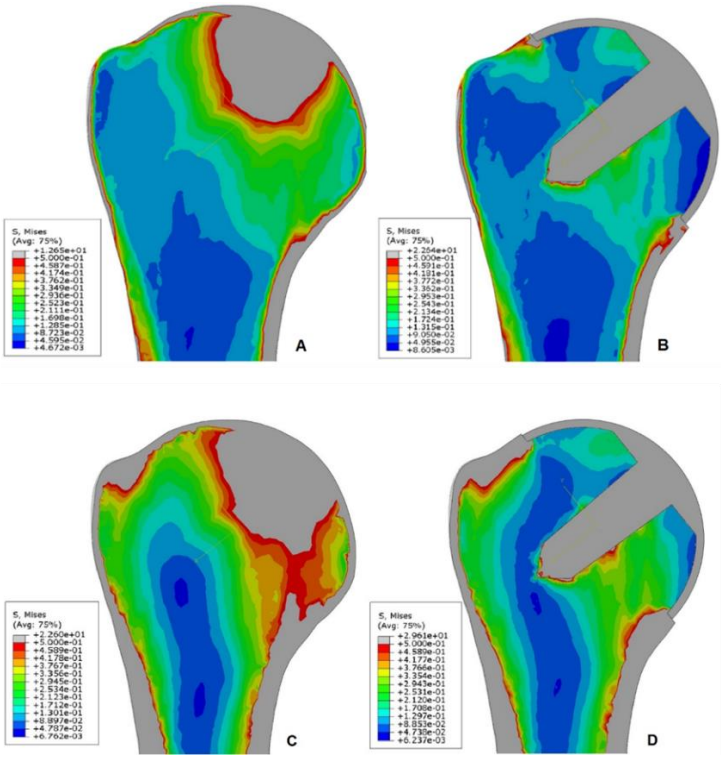

Figure 6 - Von Mises stress (MPa) distribution in the intact bone (A) and in the implanted bone with the Normal Prosthesis (B) for the flexion load case and in the intact bone (C) and in the implanted bone with the Normal Prosthesis (D) for the abduction load case.

When comparing all prostheses models, the stress distribution patterns are similar for all of them especially for these in Figures 7-A, B, and C. However, in the more superficial regions of the bone the stresses are higher for the thinner prosthesis, Figure 7-E. On the other hand, for

the larger prosthesis, in Figure 7-D, the stresses are lower in the most superficial regions of the bone.

Regarding abduction, the thinner prosthesis shows the highest stresses in the most superficial regions. The deepest regions have minor differences between all the models.

The strain energy density distribution for all the prostheses modeled, for the flexion and abduction load cases, respectively, show that the differences between the longer model and the smaller model are negligible. The thinner prosthesis shows higher strain energy density patterns in the more superficial regions of the bone, while, the larger prosthesis shows higher values of strain energy density for the more interior regions of the humeral head. Generally, all the models show higher strain energy density values than the standard prosthesis in the right lateral region of the prosthesis. The regions around the rim of the prosthesis show elevated strain energy densities for all models.

Comparison between the intact bone and the implanted bone

Figure 8 present the results for the quantitative comparison between the intact bone and the implanted bone for different prosthesis, according to Equation 3.

According to Figure 8, a clear pattern is identified for all subjects for both and all prosthesis, the four most superficial regions show the highest decreases in Von Mises stress, from the intact model to the implanted model, whereas the four deepest regions show smaller differences. The superficial regions of the humeral head (Regions 1,2,3, and 4) show a decrease between 45% and 85% in stress while the deepest regions (Regions 5,6,7, and 8) present a decrease of about 20% in stress and, in some cases, an increase. The variability in the results is wider in the regions with greater loss and it is more limited in the remaining regions.

Results regarding the strain energy density distribution have shown the same pattern and are depicted in Figure 9. Regions 1,2,3, and 4 show larger decreases in the strain energy density, from the intact bone to the implanted bone, while the other four regions show smaller differences between the models. In the deepest regions the differences are closer to zero and in some cases there is even an increase in the strain energy density.

For both measurements, most of the computed differences are negative, thus confirming the qualitative results previously presented.

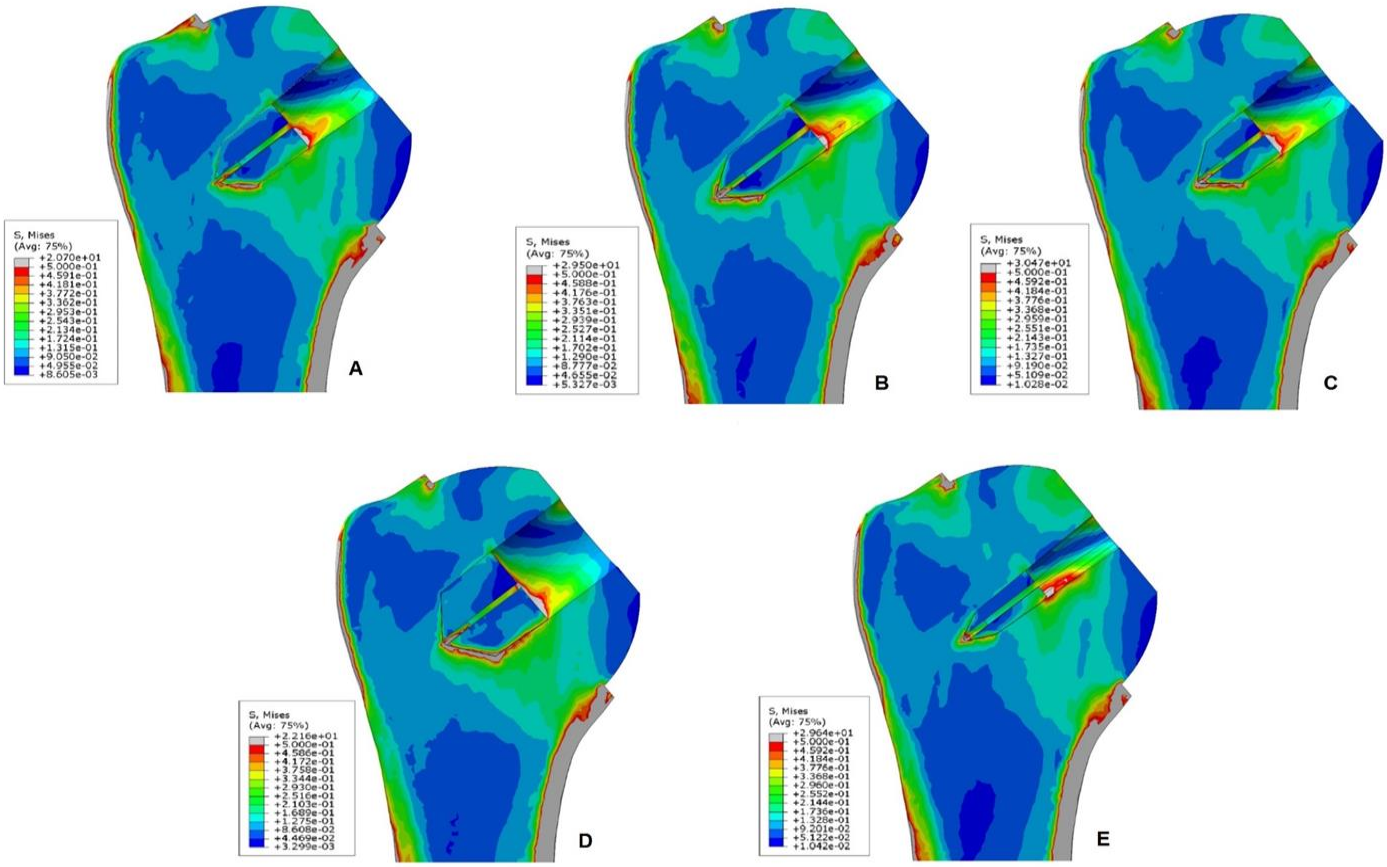

Figure 7 - Von Mises stress (GPa) distribution in the bone implanted with the Normal Prosthesis (A), the Longer Prosthesis (B), the Smaller Prosthesis (C), the Larger Prosthesis (D) and the Thinner Prosthesis (E) for a Flexion movement.

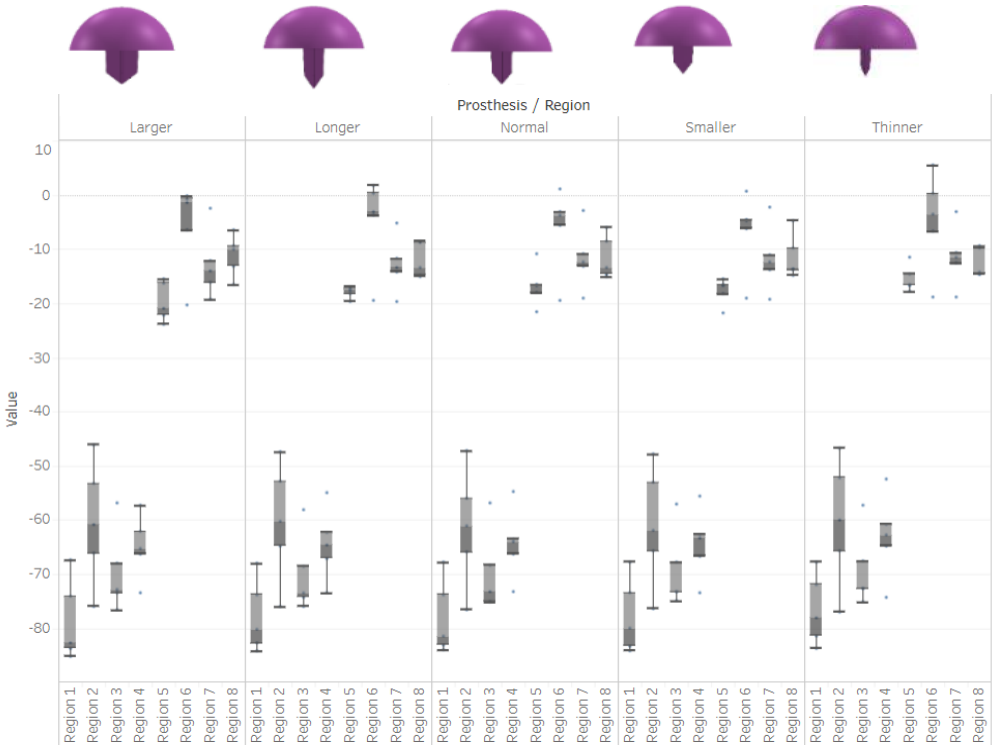

Figure 8 - Percentage (%) of change in Von Mises stress in a Flexion movement for all five subjects and for all eight regions.

Comparison between the standard prosthesis and other models

Figure 10 shows the relative difference between the modified prostheses and the standard prosthesis, in Equation 4, for the eight regions of the humerus regarding the Von Mises stress and the strain energy density, respectively.

Note that in this section, values above zero mean a decrease in the difference of stresses and strains relative to the intact bone whereas values below zero mean an increase in the difference of these stresses and strains relative to the intact bone.

According to Figure 10, the differences between the standard, longer, and smaller models were small, below 5%. More remarkable differences were observed for the larger and the thinner models. Overall, the thinner model shows an increase in the Von Mises stresses with respect to the standard model, whereas the larger model shows a decrease.

The results regarding the strain energy density are depicted in Figure 11, the largest differences are obtained for the larger and thinner models, as observed for the Von Mises stress.

The thinner model shows the biggest differences in comparison to the standard prosthesis. However, the differences between the standard and the larger prosthesis are less relevant and around 15%. In spite of the positive values in some regions showed by the larger, the thinner model seems to be the model with a closest approximation to the natural strain energy density values of the intact bone.

4. Discussion

Over the past decades, the SRA has gained popularity due to its good outcomes and decreased bone resection. However, the shoulder resurfacing has been scarcely addressed in the literature since most of the emphasis in total joint replacement research and development has been placed on the knee and hip components. The main goal of this work was to understand the influence of the characteristics of the implant on the stress distribution of the humerus after a shoulder resurfacing arthroplasty using 3D FEM.

Many manufacturers or university laboratories have been using to create designs of joint replacement prostheses. However, quantitative accuracy of these designs can never be assured because of anthropometric differences between patients (Prendergast 1997).

This work focused on the mechanical changes in stress and strain energy density due to design modifications. The closer the stress patterns in the bone are to the natural stress patterns, the less likely it is that adverse bone remodeling occurs (Ridzwan et al. 2007). According to Wolf's law, the bone will adapt to the loads under which it is placed. Hence, when a prosthesis is implanted, it tends to support the majority of load, shielding the bone from stress and compromising the natural distribution of stresses and strains (Ridzwan et al. 2007). The results provide insight to what extent this

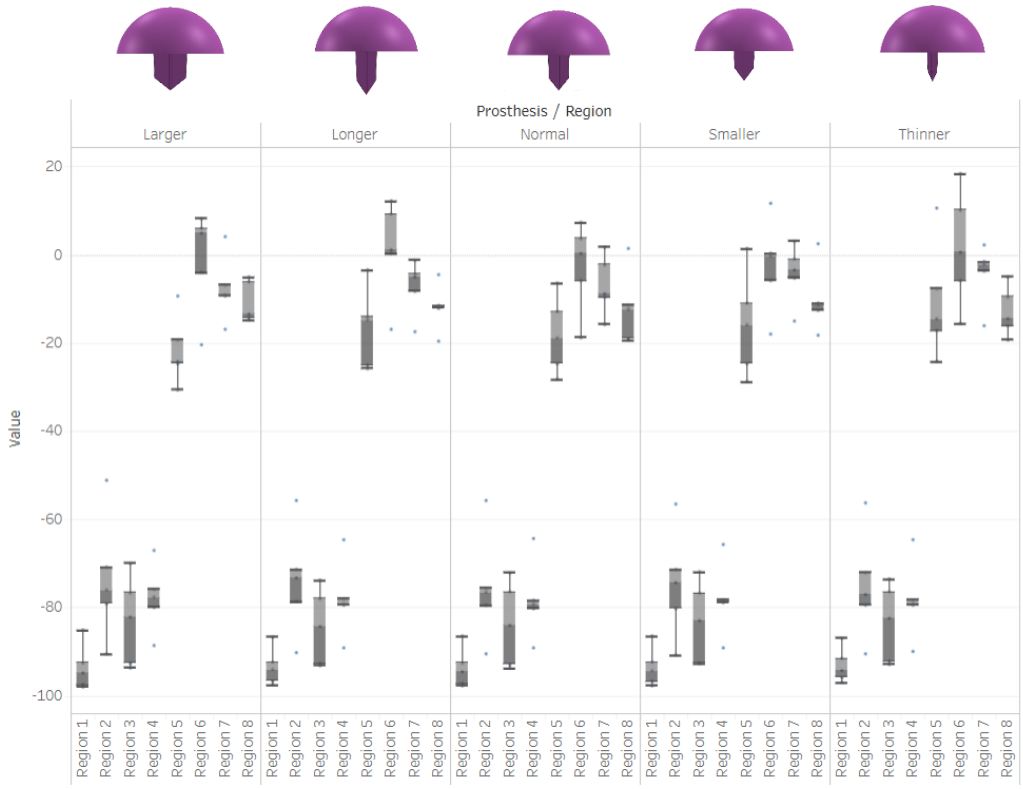

Figure 9 - Average relative difference (%) in strain energy density for the flexion load case for all five subjects and for all eight regions. The x-axis represents, on top, the prostheses modeled and, on bottom, the eight regions of the humerus defined.

phenomenon occurs and if any other design could attenuate it.

The results obtained confirmed the occurrence of the stress shielding phenomenon due to the prosthesis implantation. The results show that the largest stresses supported by the intact bone are, after the implantation, supported almost entirely by the prosthesis. The stresses below the tip of the prosthesis and below the rim, however, are closer to the intact bone condition. These results are consistent with those of Ridzwan et al. (2007) and Ong (2006), obtained while addressing the stress shielding phenomenon in a hip joint replacement.

Qualitative results did not show significant differences between prostheses models. However, in stem diameter altered models the differences are clearer. The largest differences can be seen in the most superficial regions of the bone.

Quantitative results confirm that, in fact, the regions in which the differences in stress are higher are the most superficial regions. Region 1, 2, 3 and 4 (depicted in Figure 5) of the implanted bone show a decrease in Von Mises stress and strain energy density. Quantitative results agree with qualitative results as the thinner prosthesis shows a lower decrease in Von Mises stress and strain energy density comparing to the intact bone.

Higher values of strain energy density are found in the regions around the tip and rim of the prosthesis, similarly to studies conducted on the femoral head by Gupta, New, and Taylor (2006). In the regions where the stress and strain shielding effect is higher, the thinner prosthesis is the one that better reproduces the natural anatomy of the shoulder.

A more direct comparison to the standard prosthesis is performed to understand if there is a more beneficial model. In general, models with more positive values than the standard prosthesis constitute a better option relative to the stress and strain distribution. One should take into account that, even though higher stresses represent an improvement, the increase in tension must be as smooth and homogeneous as possible and avoid localized stress peaks. The alterations in stem diameter are more significant than the alterations in stem length as qualitative results revealed. Figures 10 and 11 show that a thinner stem led to a reduced difference in the stress and strain distribution patterns between the intact bone and the implanted bone.

The numerical predictions of this study agree well with others (Gupta et al. 2006; Orr and Carter 1985; Schmidutz et al. 2014) regarding the existence of higher stress shielding effects on the most proximal regions of the bone. The results are in agreement with Schmidutz et al. (2014), i.e., they show that the SRA causes inhomogeneous stress distribution in the humeral head and induces stress shielding effect. Ong et. al (2006) described a non-physiological distribution of stresses and strains in their FE of a cemented hip resurfacing arthroplasty, revealing increased stress around the stem, also seen in this study for the humeral head. Identical results were found by Watanabe et al. (2000) showing a high degree of stress shielding in the superior femoral head. Schmidutz et al. (2014) compared the effect of the

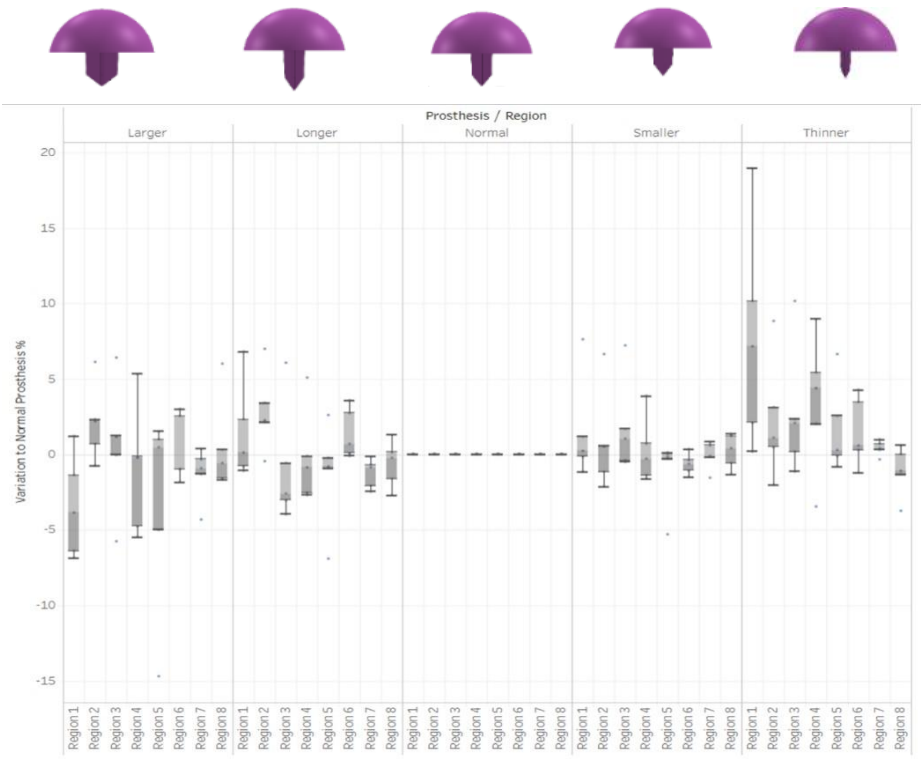

Figure 10 - Percentage (%) of change in Von Mises stress in a Flexion movement for all five subjects and for all eight regions.

stress shielding phenomenon in the bone remodeling of two fixation geometries of an SRA prosthesis. One of the models had a conical crown shaped ring and the other one had a central stem, similarly to the models considered in this work. The results presented for the SRA prosthesis with a central stem are similar to those presented in this study. The model with the conical crown ring presented a more balanced strain pattern around the stem. Schmidutz et al. (2014) also suggest that the use of stems which transfer the load to the surrounding area of the bone would be favorable. The idea is that designs with an increased stem surface should transfer the load to a larger bone stock area, thus resulting in fewer regions of unloaded bone. However, no study has ever shown this so far. In the present study, the model with the largest surface area did not present significant improvements on the stress or strain distribution patterns when compared to the standard model. Unfortunately, there is still little numerical studies available in literature on the shoulder resurfacing arthroplasty consequences on the stress and strain patterns, especially for different types of prostheses. Most of the studies concern the glenoid component design, as the main issue reported with the SRA is glenoid component loosening (Wirth and Rockwood Jr. 2017).

In this study, the prosthesis with the thinner stem showed the most potential in reproducing the natural load patterns in the humerus. However, note that other critical factors for the success of the SRA such as mechanical stability, may compromise the performance of the thinner model. Future studies should address also other critical factors besides stress shielding phenomenon.

The present work overcomes some limitations of previous studies. The main strength of this study is the evaluation of five anatomically different subjects, while previous studies neglected interpatient densitometric and geometric variation (Orr and Carter 1985; Schmidutz et al. 2014). This study considered the action of muscular forces, usually ignored in other studies, for two arm positions. The study of different stem diameter and length prostheses constitutes an innovative approach to the study of the influence of the prosthesis' parameters in the stress shielding effect in the SRA.

Despite the strengths of this study, it is not without limitations. Firstly, the segmentation and the geometry creation processes are susceptible to error and may cause geometric changes in the bone natural morphology. Secondly, the densitometric conditions computed from the CT scans constitute pre-operative conditions. Moreover, the assignment of density values to the mesh may also lead to incoherencies. The size and location of the muscle insertions for each subject relied on personal judgement along with literature information. Another concerning aspect is the modification considered to for the prostheses. The stem was changed in 25% of its width and length which might not induce such a significant change in stress and strain patterns. Regarding the contact definition, it is still not clear in literature which friction coefficient simulates better the contact between the bone and the implant. The coefficient chosen was the most usually cited. The evaluation of more load cases, especially of daily activities, would be beneficial. It would be interesting if this work considered,

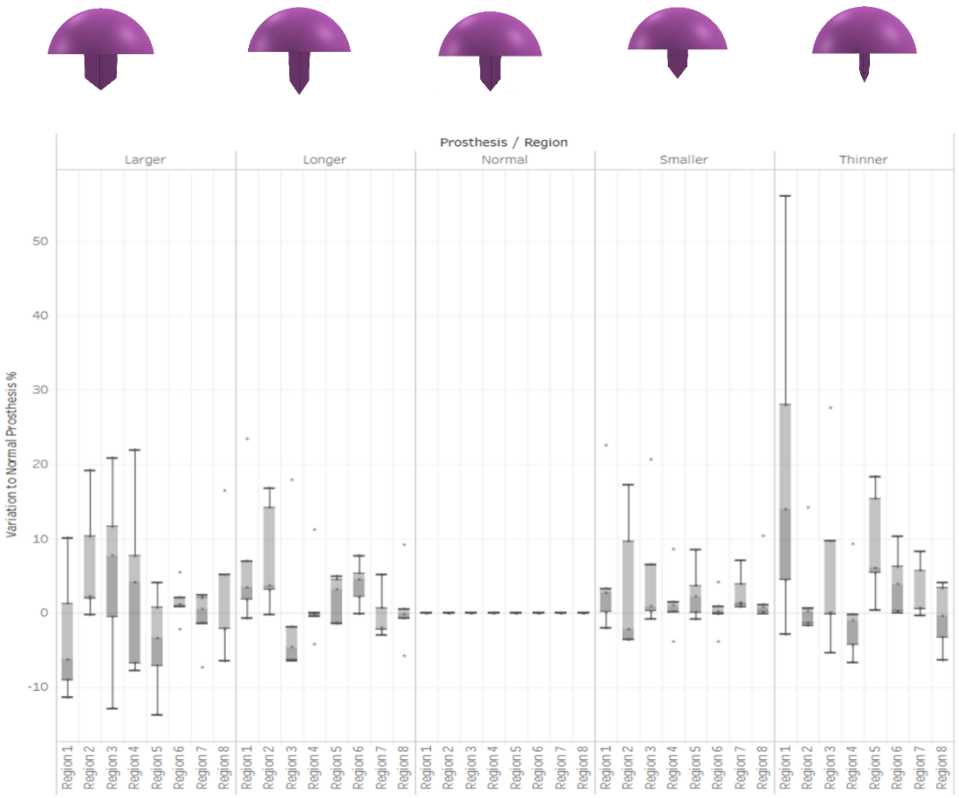

Figure 11 - Average relative difference in strain energy density (%) between the standard and modified models for the flexion load case. The x-axis represents, on top, the prostheses modeled and, on bottom, the eight regions of the humerus defined.

as well, the bone remodeling process to understand deeply the changes in bone density with each model.

In summary, despite the scarce number of studies addressing the SRA, the results of the stress distribution patterns are in agreement with previous ones. The decrease in stem diameter shows potential to reduce the stress shielding effect. However, other critical factors such as stability, also need to be studied. Despite the limitations of this work, this study is expected to provide relevant insight into the influence of different parameters of the SRA prostheses on the stress and strain distribution patterns in the humerus.

Conclusions and Future Developments

The current work studied the influence of the characteristics of the resurfacing prostheses on the stress distribution patterns after a shoulder resurfacing arthroplasty. The width and length of the prosthesis stem were changed and five prostheses models were evaluated: the standard model, two models with a larger and a thinner stem, and two models with a longer and a smaller stem. Five anatomically distinct subjects were implanted with the five models, which resulted in a total of thirty finite element simulations. The Von Mises stress and the strain energy density were evaluated for all.

A comparison between the intact bone and all the models revealed the existence of the stress shielding phenomenon for the implanted bone, which is in agreement with previous studies. When comparing the different prosthesis models, the model with the thinner stem showed the most potential in distributing stresses in a closer way to the natural anatomy. However, a thinner stem might implicate stability issues that must be addressed in future studies.

Despite the many strengths of this study, further studies are needed to deepen the knowledge regarding the consequences of the SRA. Ideally, future studies should combine the stress shielding effect analyses with bone remodeling algorithms to understand how the design of resurfacing prostheses influences these events. The current study presents some dispersion in the result, which limited its findings. This dispersion is mainly due to anatomical differences, accentuated by the lower number of subjects. Future studies should combine prosthesis' parameters modification, for instance, models with smaller and larger stems, or longer and larger stems, among others.

It would be interesting to determine clusters of subjects characterized by its size and assign each cluster to a suitable prosthesis model that would probably differ according to the clusters' characteristics. It is known that the positioning of the resurfacing prostheses constitutes a main issue for surgeons (Ryan et al. 2015). This difficulty might lead to wrong positioning and consequently harm stress and strain distribution patterns. Future studies should also focus on the influence of the positioning of the resurfacing prostheses on shoulder arthroplasty.

In conclusion, the results of this study represent a relevant contribution to the understanding of the consequences of the implant on the mechanical outcome of the SRA.

References

DePuy Synthes. 2017. “GLOBAL® CAP and GLOBAL® CAP CTA™ Shoulder Systems | DePuy Synthes Companies.” Retrieved June 19, 2017 (https://www.depuysynthes.com/hcp/shoulder/products/qs/GLOBAL-CAP-and-GLOBAL-CAP-CTA).

Gupta, Sanjay and Prosenjit Dan. 2004. “Bone Geometry and Mechanical Properties of the Human Scapula Using Computed Tomography Data.” Trends Biomater Artif Organs 17(2):61–70.

Gupta, Sanjay, Andrew M. R. New, and Mark Taylor. 2006. “Bone Remodelling inside a Cemented Resurfaced Femoral Head.” *Clinical Biomechanics* 21(6):594–602.

Ong, K. L. 2006. “Biomechanics of the Birmingham Hip Resurfacing Arthroplasty.” *Journal of Bone and Joint Surgery - British Volume* 88–B(8):1110–15.

Orr, T. E., D. R. Carter, and D. J. Schurman. 1988. “Stress Analyses of Glenoid Component Designs.” *Clin.Orthop.Relat Res.* (0009–921X (Print)):217–24.

Quental, C., Folgado J., Ambrósio J., and Monteiro J. 2013. “Multibody System of the Upper Limb Including a Reverse Shoulder Prosthesis.” *Journal of Biomechanical Engineering* 135(11):111005.

Ribeiro, N. S., Fernandes P. C., Lopes, D. S., Folgado. J. O., and Fernandes, P. R. 2009. “3-D Solid and Finite Element Modeling of Biomechanical Structures - a Software Pipeline.” in 7th EUROMECH Solid Mechanics Conference.

Ridzwan, M. I, Solehuddin Shuib, A. Y. Hassan, A. A. Shokri, and M. N.Mohamed Ibrahim. 2007. “Problem of Stress Shielding and Improvement to the Hip Implant Designs: A Review.” *Journal of Medical Science* 460–67.

Ryan, P., C. Anley, A. Lambrechts, B. Vrettos, and S. Roche. 2015. “Technical Difficulty in Component Sizing and Positioning in Humeral Resurfacing: Relationship to Clinical Outcomes.” *The South African Orthopaedic Journal (SAOJ)* 14(3):32–42.

Schmidutz, F., Agarwal, Y., Müller, P. E., Gueorguiev, B., Richards, R. G., and Sprecher, C. M. 2014. “Stress-Shielding Induced Bone Remodeling in Cementless Shoulder Resurfacing Arthroplasty: A Finite Element Analysis and in Vivo Results.” *Journal of Biomechanics* 47(14):3509–16.

Watanabe, Yuichi, Shiba, Naoto, Matsuo, Shigeaki, Higuchi, Fujio, Tagawa, Yoshihiko, and Inoue, Akio 2000. “Biomechanical Study of the Resurfacing Hip Arthroplasty.” *The Journal of Arthroplasty* 15(4):505–11.

Wirth, M. A. and C. A. Rockwood Jr. 2017. “Complications of Shoulder Arthroplasty.” *The Journal of Bone and Joint Surgery* 99(307):47–69.